Hindawi
Mathematical Problems in Engineering
Volume 2019, Article ID 3712012, 19 pages
https://doi.org/10.1155/2019/3712012

Research Article

Experimental Investigation of the Effect of Ice Blockage on Propeller Hydrodynamic Performance

Chun-Yu Guo, Pei Xu, Chao Wang, and Wei-Peng Xiong

College of Shipbuilding Engineering, Harbin Engineering University, Harbin 150001, China

Correspondence should be addressed to Chao Wang; wangchao806@hrbeu.edu.cn

Received 2 October 2018; Accepted 13 December 2018; Published 3 January 2019

Academic Editor: Fausto Arpino

This experimental study investigates the influence of different sizes, quantities, and axial positions of model ice on propeller hydrodynamic performance. We used particle image velocimetry measurements to analyze the characteristics of the propeller wake flow field. The measurement results show that ice blockage leads to an increase in propeller thrust, torque, and efficiency. The smaller the advance coefficient of the propeller is, the smaller the influence of model ice on propeller blockage is. As the model ice becomes thicker and the thrust and efficiency of the propeller increase, the propeller torque is smaller for low advance coefficient and higher for high advance coefficient. The wider the model ice is, the larger the thrust and torque of the propeller are. Once the model ice width exceeds the propeller diameter, the change in its width has no effect on propeller efficiency. When the propeller is blocked with model ice, the fluid velocity in the wake flow reduces in the inflow direction, and the increase in fluid velocity in the horizontal transverse direction and variation of fluid velocity in the vertical direction are related to the model ice width.

1. Introduction

The occurrence of global warming is increasing the possibility of northern shipping routes being opened, and the commercial value of the Arctic channel is likely to continue increasing. Furthermore, the area surrounding the North Pole is rich in natural resources such as petroleum, natural gas, and coal. Ice-going ships are expected to play an increasingly important role in resource exploration, development, transportation, and scientific research in the low-temperature, icy, and extremely challenging Arctic climate. Because of the variable conditions under which ice-going ships operate, the working environments of their propulsion devices are considerably different from those of conventional ships. In particular, under ice-breaking conditions, brash ice frequently slides to the bottom surface of the ship and then into the flow field in front of the propeller. This induces extreme loads on the propeller blade and in turn influences the propeller hydrodynamic performance and causes serious noise, vibration, and cavitation problems. Therefore, research on propeller-ice interaction is of great significance.

Previous studies on propeller-ice interaction have reported valuable findings. The law and mechanism of propeller-ice interaction have been obtained preliminarily, and experimental measurements are usually used. Lindroos and Bjorkestam [1] were the first to successfully use a flat plate to represent an ice blockage in a propeller test. Their work was subsequently advanced by Shpakoff and Segrecrantz, who were the first to explore the effect of hydrodynamic loads on the propeller for the change in distance between the blockage and the propeller blades [2]. Luznik et al. [3] measured the change in the propeller hydrodynamic performance for different advance coefficient values with fixed clearance between the propeller blades and the blockage. Other studies have assessed the propeller hydrodynamic performance for different clearances between the blockage and the propeller blades with fixed advance coefficient. Newbury et al. [4, 5] performed a similar test, but for different model configurations. Walker [6] found that a blockage resulted in an increase in the thrust, torque, and average load vibration. Moores et al. [7] performed experiments for a highly skewed propeller in an ice tank, explored the variation in the propeller thrust and torque with the advance coefficient, and observed the extent of damage to the propeller blade. Sampson and Atlar [8, 9] performed a test to examine the performance of a podded ice-class propeller operating at variable distances from an ice

blockage. The propeller hydrodynamic performance became insensitive to the increase in the milling depth and sensitive to the change in clearance between the propeller and the ice, and cavitation caused serious erosion. Wang [10] performed a series of tests in an ice tank and found that propeller-ice interaction loads mainly depended on the propeller shape and the operating conditions (e.g., advance coefficient, angle of attack, and depth of milling). In the aspect of theory, Shih et al. [11] used a three-dimensional panel method to examine the increases in thrust and torque for fixed distance between the blockage and the propeller. Liu et al. [12–14] developed an unsteady three-dimensional surface panel method to successfully forecast hydrodynamic load fluctuations on an ice-class propeller and also developed a method for the design and optimisation of the strength and integrity of ice-class propellers. Wang [15] used the viscous flow theory to forecast the hydrodynamic performance of ice-class propeller and flow characteristics in blockage conditions. In terms of flow field measurement, Walker [16] and Atlar [17] measured the flow velocity behind model ice by using laser Doppler velocimeter (LDV) and explained the flow state of the fluid in the area of propeller operation. The results indicated that, in the presence of model ice, the induced velocity field decreased both in front of and behind the propeller disk.

However, in previous studies on propeller-ice interaction, model ice was limited to only a single type. In-depth investigations have not yet been conducted with different widths, thicknesses, and number of ice pieces and on the wake field of the propeller in the blocked flow. To address these deficiencies, an experiment was performed to study the effect of synthetic ice on the propeller hydrodynamic performance in the towing tank at Harbin Engineering University in China. The propeller hydrodynamic performance was assessed by varying the width, thickness, and number of pieces of model ice as well as by using a range of clearances between the model ice and the propeller blades. Simultaneously, the accurate particle image velocimetry (PIV) measurement technique was used to analyze the flow field under propeller blockage conditions.

2. Test Facilities

2.1. Experimental Setup. The experiment to test the effect of model ice blockage on the propeller hydrodynamic performance was conducted in the towing tank at Harbin Engineering University. The size of the ship model towing tank is 108 × 7 × 3.5 m (length × width × height), and the steady velocity range of the trailer is 0.1–6.5 m/s. The experimental equipment mainly consisted of the propeller open-water device and a driver-controlled ice-feeding mechanism. The ice-feeding mechanism allowed for a controllable advancing speed and a precise moving distance. The accuracies of the velocity and displacement of the model ice are ± 0.01 mm/s and ± 0.01 mm, respectively, and the maximum moving distance is 550 mm. The outer side of the ice-feeding mechanism is equipped with an airfoil, which effectively reduces the surface wave generated by the device near the water surface. The propeller open-water device mainly includes a dynamic signal testing and analyzing system, propeller dynamometer, motor, and open-water test boat. The range of the dynamic signal testing and analyzing system is ±20 mV to ±20 V, and the maximum sampling frequency is 20 kHz. In this experiment, the sampling frequency was set to 200 Hz, and the sampling time was 30 s for the uniform velocity measurement section. The chosen sampling frequency fully considers the shedding frequency of the model ice wake vortex, and the shedding frequency of the model ice wake vortex was mainly analyzed by CFD numerical simulation software [15]. The rated torque and thrust of the propeller dynamometer are 10 Nm and 250 N, respectively, and the maximum speed is 3500 rpm.

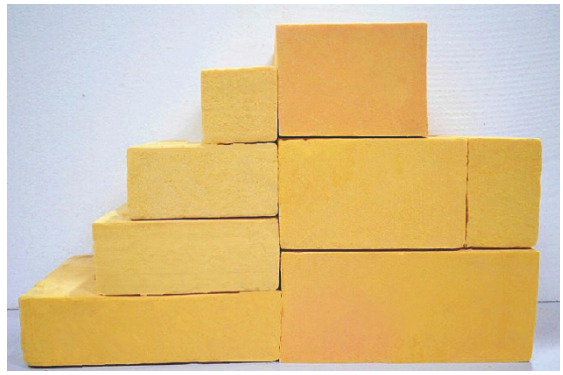

Figure 1: The model ice with different sizes.

2.2. Model Ice. Considering the restrictions of the ship model towing tank and experimental devices, actual freezing ice could not be used as the experimental material in the test process; therefore, phenolic foam panels were used to simulate ice. Compared to freezing ice, synthetic ice has the advantages of being low cost, having a short production time, and exhibiting stable properties. Figure 1 shows the model ice used in the experiment. The model ice length is L = 200 mm; the widths are B = 80, 160, 200, and 280 mm; and the thicknesses are H = 80 and 120 mm.

2.3. Propeller Model. The propeller used in the experiment was a $1/6^{th}$ scale model of the prototype propeller. Table 1 lists the relevant dimensions and parameters of the propeller model.

2.4. Underwater PIV System. To better understand the propeller's wake flow information in blocked flow, an accurate three-dimensional underwater PIV measurement technique was used to trace the flow field around the propeller in this experiment. The three-dimensional velocity field components, including the turbulence characteristics, vortex, and flow separation, were obtained simultaneously by using the three-dimensional PIV technique. Table 2 shows the performance indicators of the PIV measurement system.

3. Test Data Analysis

The relative coordinate system of the model ice motion was established, as shown in Figure 2. The origin (o) of the

Table 1: Principal dimensions of propeller model.

Conventional propeller			
Diameter (mm)	150	Number of blades	4
Rake(°)	10	Type	MAU
Blade area ratio	0.7	Direction of rotation	Left
Pith ratio(0.75R)	0.807	Material	Aluminium
Hub ratio	0.18	Scale	$\lambda = 6$
r/R	C/D	T/D	P/D
0.2	0.2635	0.0406	0.807
0.3	0.3077	0.0359	0.807
0.4	0.3448	0.0312	0.807
0.5	0.3736	0.0265	0.807
0.6	0.3925	0.0218	0.807
0.7	0.3946	0.0171	0.807
0.8	0.3680	0.0124	0.807
0.9	0.2915	0.0077	0.807
1	0.0685	0.0003	0.807

Table 2: Performance index of PIV measurement system.

PIV system parameter	
CDD resolution(pixels)	2048 × 2048
Laser beam duration(ns)	4
Laser wavelength(nm)	532–1064
PIV tracer	Polyamide particles (PSP-50μm)
Pulsed laser sheet thickness(mm)	0.6
Maximum measurement range(mm)	400 × 400
PIV data processing software	Dantec Dynamic Studio V3.41
Maximum laser pulse energy(MJ)	120

coordinate system is fixed at the front end of the propeller blade, the x-axis points in the inflow direction, the y-axis points toward the left (when viewed from the propeller shaft toward the inflow direction), and the positive direction of the z-axis is upward according to the right-hand rule. During the experiment, the plane of the model ice closest to the propeller is considered to be the reference plane, and the midpoint of the lower line of the reference plane is considered to be the reference point that can be used to adjust the model ice to different locations. In addition, the blockage height of the model ice on the propeller is denoted by h, and $h = R - R_h - z_i$, where $R = 75$ mm is the propeller radius, $R_h = 15$ mm is the propeller hub radius, and i is the model ice reference point. When the model ice thickness is $H = 80$ mm, the coordinate is $z_i = 5$ mm, and the blockage height is $h = 55$ mm. When the model ice thickness is $H = 120$ mm, the coordinate is $z_i = -35$ mm, and the blockage height is $h = 95$ mm. Figure 2 also shows the blockage height, reference point, and thickness and width of the model ice, and the direction of the arrowhead is the direction of the propeller's rotation (when viewed from the propeller shaft toward the direction of inflow). V_A is the inflow velocity.

The propeller rotational speed is set to n =1000 rpm in consideration of factors including the length of the towing tank, trailer velocity, Reynolds number, and testing water temperature of 15°C. The Reynolds number of the propeller blade, $R_e = 3\times10^5$, as calculated according to Eq. (1) met the requirements specified by the ITTC performance committee, and the propeller is in the state of turbulent flow [18]. The immersion depth of the propeller shaft is 2D, which meets the requirements of the ITTC specification for appropriate immersion depth ($h_s \geq 1.0D$) of the propeller shaft. The influence of surface wave generated by the ice-feeding mechanism on hydrodynamic performance of the propeller is thus effectively avoided [19].

During the experiment, the thrust and torque of the propeller were measured by a propeller dynamometer. To analyze and compare the experimental results, the dimensionless coefficients are defined as given by (2), (3), (4), and (5).

$$\text{Reynolds number: } R_e = \frac{b_{0.75R}\sqrt{V_A^2 + (0.75\pi nD)^2}}{\nu} \quad (1)$$

where $b_{0.75R}$ is the section chord length of the propeller blade at 0.75R, n is the propeller rotational speed, D is the propeller diameter, and υ is the kinematic viscosity coefficient of water.

$$\text{Thrust coefficient: } K_T = \frac{T}{\rho n^2 D^4} \quad (2)$$

$$\text{Torque coefficient: } K_Q = \frac{Q}{\rho n^2 D^5} \quad (3)$$

$$\text{Propeller efficiency: } \eta = \frac{K_T}{K_Q}\cdot\frac{J}{2\pi} \quad (4)$$

$$\text{Advance coefficient: } J = \frac{V_A}{nD} \quad (5)$$

where K_T and K_Q are the thrust and torque coefficients, respectively; T, Q, and η are the propeller thrust, torque, and efficiency, respectively; J is the advance coefficient; ρ is the density of water; and the other parameters are as defined previously.

3.1. Propeller Open-Water Test. Figure 3 shows the open-water performance curve of the propeller thrust, torque, and efficiency as a function of the advance coefficient, in the range of $J = 0$–0.9.

3.2. Analysis of Propeller Hydrodynamic Performance for Different x-Axis Positions of Model Ice. This section discusses the results of model ice with size of 200 × 200 × 80 mm. The coordinates of the model ice on the y- and z-axes are $y_i = 0$ mm and $z_i = 5$ mm, respectively. These coordinates are used to explore the change in the propeller hydrodynamic performance at different distances between the propeller and the model ice when the propeller is operated under different advance coefficients of $J = 0.2$, 0.4, and 0.7 and when the range of motion of the model ice is $X = 1$–500 mm. Figure 4 shows the installation position of the propeller and model ice. Figure 5 shows the measurement results.

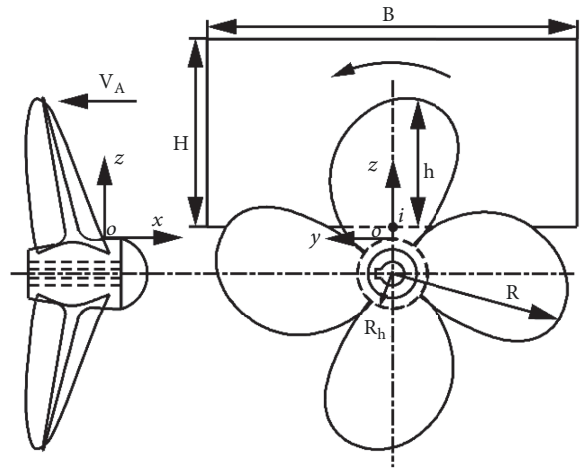

Figure 2: *O-xyz* coordinate system and the correlation definition of model ice and propeller.

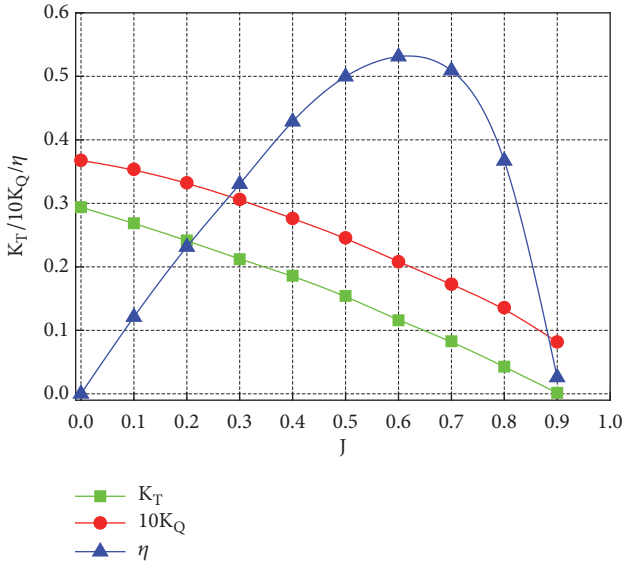

Figure 3: Propeller open-water performance curve.

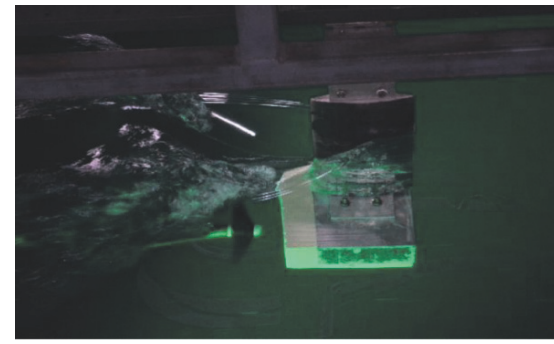

Figure 4: Installation position of propeller and model ice (X = 200 mm).

Figures 5(a) and 5(b), respectively, show the propeller thrust and torque coefficient curves for different distances between the propeller and the model ice; the values of the thrust and torque coefficients in uniform flow for the same advance coefficient are plotted as horizontal lines. The figures show that the propeller thrust and torque increased with ice blockage. Furthermore, the propeller thrust and torque increased gradually as the distance between the propeller and the model ice decreased from 500 to 10 mm. The thrust and torque continued to increase when the distance was less than 10 mm but exhibit a "shaky" behaviour, indicating unstable performance probably due to the flow separation behind the blockage close to the propeller [16]. There are two main reasons for the increase in propeller thrust and torque as the distance between the propeller and the model ice decreased. The first is due to the blockage effect of the model ice on the incoming flow that reduces the inflow velocity at the front of the propeller and causes a low advance coefficient. The second is the wall effect (or boundary effect) appearing in the high-speed wake zone that causes increased inflow field velocity between the propeller and model ice [5, 12]. The propeller thrust and torque are a nonlinear function of the distance between the propeller and the model ice. During blockage, the hydrodynamic load of the propeller mainly comprises two types of flow: conventional uniform flow of the propeller blades without occlusion and disturbance flow (turbulent and separated flow) generated when the propeller blades are subjected to wake turbulence caused by the model ice. The latter type of flow is the main cause of the increase in the propeller thrust and torque.

To analyze the relationship between the degree of blockage and the advance coefficient, the amplification of propeller thrust and torque coefficients during ice blockage relative to open-water values is calculated, where the amplification

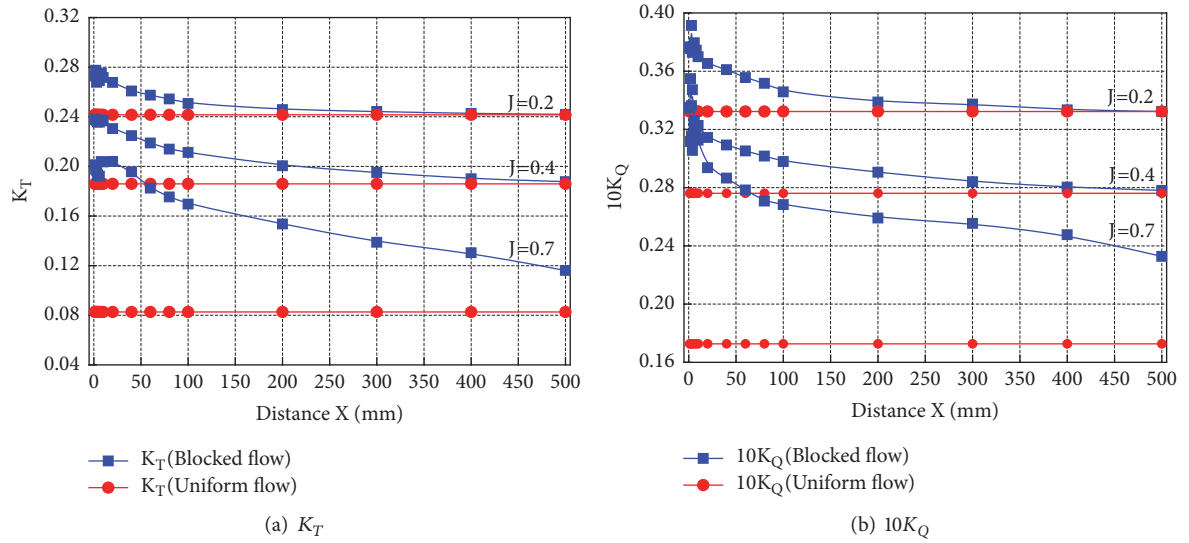

Figure 5: Variation of propeller thrust and torque coefficients in varying proximity of the propeller to the model ice.

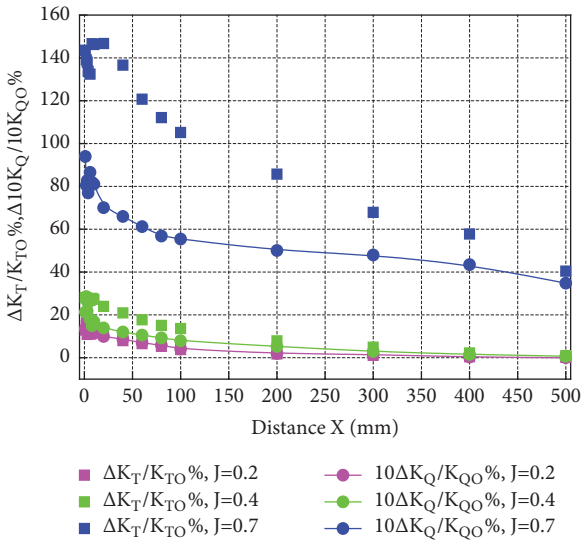

Figure 6: Variation of amplification of propeller thrust and torque coefficients in varying proximity of the propeller to the model ice.

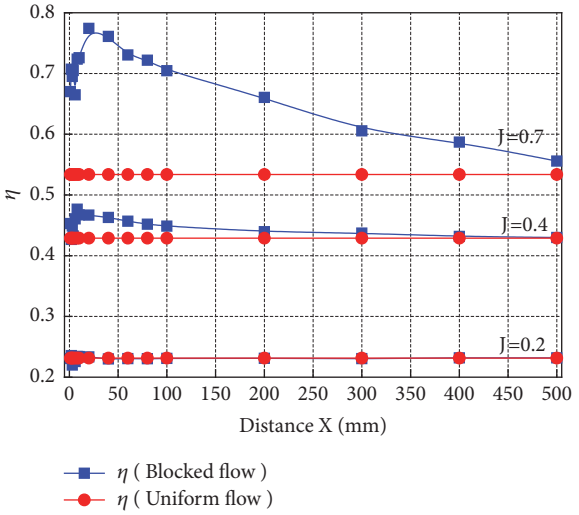

Figure 7: Variation of propeller efficiency in varying proximity of the propeller to the model ice.

of the propeller thrust coefficient is defined as $\Delta K_T / K_{TO}\%$, where $\Delta K_T = K_{TB} - K_{TO}$, K_{TB} is propeller thrust coefficient under the blockage, and K_{TO} is propeller thrust coefficient in open-water. The amplification of the propeller torque coefficient is defined as $\Delta 10K_Q/10K_{QO}\%$, where $\Delta 10K_Q = 10K_{QB} - 10K_{QO}$, $10K_{QB}$ is propeller torque coefficient under the blockage, and $10K_{QO}$ is propeller torque coefficient in open water. As shown in Figure 6, the degree of ice blockage and the advance coefficient have a nonlinear positive correlation. In other words, with an increase in the advance coefficient, the amplification of the propeller thrust and torque coefficients in blockage conditions also increase. Furthermore, the greater the inflow velocity, the greater the amplification of the propeller thrust and the torque coefficients. For advance coefficient of $J = 0.2$, the amplification of the propeller thrust coefficient is slightly smaller than that of the torque coefficient during blockage. For advance coefficient of $0.4 \leq J \leq 0.7$, the amplification of the propeller thrust coefficient is much greater than that of the torque coefficient during blockage, especially for $J = 0.7$. At that level, the maximum amplification of the propeller thrust coefficient can be up to 140%, whereas the amplification of the torque coefficient is less than 100%. This is mainly due to the inflow velocity being larger with high advance coefficient and the blockage effect of ice being more obvious. Therefore, the propeller inflow velocity decreases more, attack angle of the blade airfoil increases, and the lift and resistance increase, and in fact, lift increases significantly.

Figure 7 shows curves representing the change in propeller efficiency with different advance coefficients. For propeller advance coefficient of $J = 0.2$, the efficiency curve of

the propeller under the blockage varies in a manner similar to that of the propeller in open water. For X = 1–10 mm, the efficiency curve is unstable in a manner similar to the tendency of the propeller thrust and torque. For advance coefficient of $0.4 \leq J \leq 0.7$, the efficiency of the propeller under the blockage is greater than that of the propeller in open water. A decrease in the distance between the propeller and the ice causes the propeller efficiency to first increase and then decrease, following which it tends to be unstable for X = 0–500 mm. Meanwhile, the propeller efficiency shows that the difference between the efficiencies of the blocked and unblocked propeller increases as the advance coefficient increases. This behaviour is mainly attributed to the efficiency being determined by the thrust and torque, and the variable amplification of the thrust and torque coefficients are both large when the advance coefficient is high. This trend is consistent with the conclusions drawn by Luznik and Wang [3, 20]. Although the propeller efficiency increases in blocked flow, the efficiency of the ship's general propulsion system may be reduced [7]. In addition, the flow field in front of the propeller is more turbulent when the propeller operations in blocked flow; this intensifies propeller cavitation, noise, vibration, and excitation force [9, 21], resulting in the erosion of the propeller blades and damage to the propeller shaft [16, 22]. Therefore, in practical application process, it is not advisable to adopt a method that involves intentionally blocking the propeller to improve propeller efficiency.

3.3. Analysis of Propeller Hydrodynamic Performance for Different Model Ice Thicknesses. To investigate the influence of different model ice thicknesses on propeller hydrodynamic performance, model ice sets with two thicknesses and four widths were selected as reference objects. The length of the model ice is 200 mm, thicknesses are 80 and 120 mm, and widths are 80, 160, 200, and 280 mm. The locational coordinates of the model ice are x_i = 20 mm, y_i = 0 mm, and z_i = 5 mm (H = 80 mm) and z_i = -35 mm (H = 120 mm), and the blockage heights of the model ice on the propeller are 55 and 95 mm. Figures 8 and 9 show the measurement results.

Figures 8 and 9 show that during blockage with varying model ice thicknesses, the propeller thrust and torque coefficients change with the advance coefficient. Figure 8 shows that, for low advance coefficient, the influence of model ice thickness on propeller thrust is not obvious. As the advance coefficient and model ice thickness increase, so does the thrust; furthermore, the increase in the advance coefficient causes the thrust difference between the two blocking states to increase. The main reason for the thrust increase is that increasing model ice thickness increases the blockage area. The blockage decreases the propeller inflow velocity, leading to an increase in thrust. Figure 9 shows that, for low advance coefficient, thicker and thinner model ice, respectively, have smaller and larger impact on propeller torque. At high advance coefficient, however, the effect of model ice on propeller torque is the opposite to the low advance coefficient. This shows that the increasing trend of propeller thrust and torque differs with model ice thickness. To further analyze the primary causes of the phenomenon, two model ice blockages of 200 × 200 × 80 mm and 200 × 200 × 120 mm were selected as the research object. By using computational fluid dynamics (CFD) software, the influence of these two blockages on the propeller hydrodynamic performance was calculated by using overlapping grid technology, as in Wang [15]. In the CFD numerical simulation, the coordinates of the model ice were the same as those in the experiment, and the advance coefficient of the propeller was J = 0.3 and 0.8. The velocity vector chart of the cross section flow field between the propeller and the ice blockage was extracted from the simulation results, and the cross section position is X = 10 mm. Figure 10 shows the velocity vector chart of the cross sectional flow field; the flow field direction is viewed from the propeller toward the inflow direction.

Figures 10(a) and 10(b) show that, for low advance coefficient, a vortex is produced between the propeller and the model ice owing to the blockage effect; furthermore, and the thicker the model ice, the larger the vortex region. The existence of the vortex region reduces the inflow velocity in front of the propeller, and the velocity gradient around the propeller blade decreases. This decrease results in a reduction in the shear stress on the propeller, implying that the friction resistance of water impact on the propeller is reduced. The main reason for the propeller torque is the combined action of the shape resistance and the friction resistance [23], and the friction resistance is the main factor affecting the propeller torque because the shape resistance is constant during rotation. Therefore, reducing the frictional resistance reduces the propeller torque, resulting in the phenomenon of smaller propeller torque with thicker model ice. Figures 10(c) and 10(d) show that, for higher advance coefficient, there is no vortex between the propeller and the model ice, and the inflow velocity around the propeller blade is relatively higher along with the shear stress and torque of the propeller. Moreover, the thicker the model ice, the greater the disturbance region of the propeller and the greater the propeller torque. This results in the phenomenon of greater propeller torque at high advance coefficients with thicker model ice.

Figure 11 shows that model ice of different thicknesses has minimal effect on the propeller efficiency for low advance coefficients and that the propeller efficiency is almost equal to that in open water. As the advance coefficient increases, the thicker the model ice, the greater the effect on propeller efficiency. For 80 mm model ice width, the efficiency of the blocked propeller linearly increases and then decreases gradually, and the change trend is similar to the efficiency curve of the propeller in open water. For model ice width of 160 mm $\leq B \leq$ 280 mm, the propeller efficiency under blockage shows a linear increasing trend, and the propeller efficiency exceeds 90%. These experimental results are similar to the literatures [3, 6, 20].

To further analyze the phenomenon of the propeller efficiency increasing gradually with the advance coefficient, consider the amplification curves of the thrust and torque coefficients shown Figures 8(c) and 9(c), respectively. The calculation is similar to that used in Figure 6, and the resulting curves are shown in Figure 12. The figure shows that the amplification of the thrust coefficient is much larger than that of the torque coefficient. In particular, when the advance

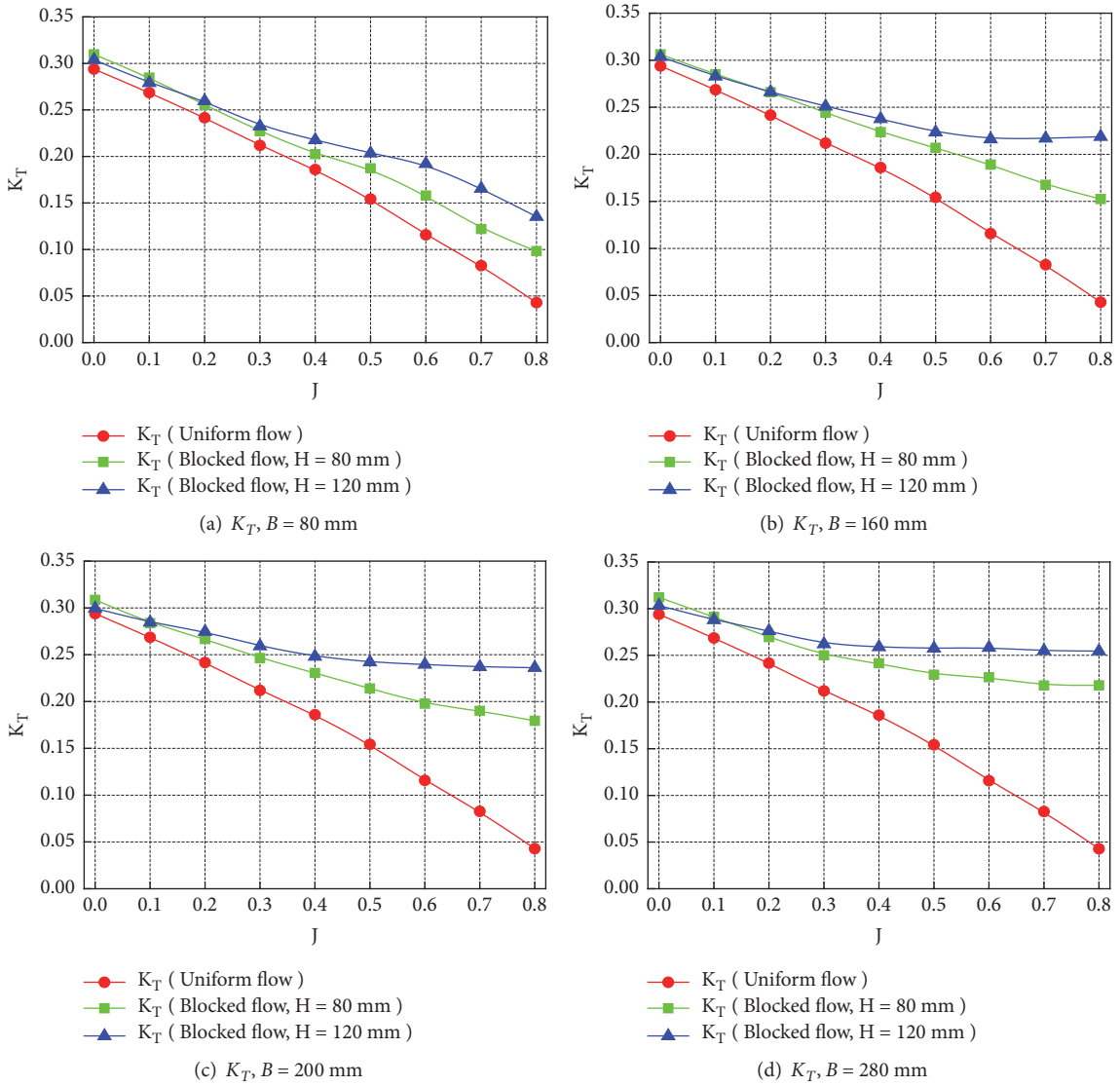

Figure 8: Variation of propeller thrust coefficient with different model ice thicknesses.

coefficient is high, the maximum amplification of the thrust coefficient under blockage can reach more than 450%, and the maximum amplification of the torque coefficient is 120%. Therefore, the efficiency increase is considered to mainly result from the significant increase in thrust. In addition, when calculating the propeller efficiency, the phenomenon of exaggerated inflow velocity in front of the propeller is seen. When calculating the open-water efficiency of a propeller, according to Eqs. (4) and (5), $\eta = K_T/K_Q \bullet J/(2\pi) = K_T/K_Q \bullet V_A/(2\pi nD)$, where V_A is the propeller advance speed or trailer velocity. However, when the propeller is blocked with model ice, the flow velocity in front of the propeller is lower than that when the propeller is unblocked. In other words, the inflow velocity in front of the propeller is less than the trailer velocity. At the same time, the flow field before the propeller is more turbulent, and the fluid velocities in the blocked and nonblocked areas are very different. It is impossible to determine the actual velocity in front of the propeller by using the current testing technique. Therefore, the propeller efficiency in the blockage test is calculated by selecting the trailer velocity. Therefore, the trailer velocity as inflow velocity in front of the propeller also leads to increased propeller efficiency in the calculation process.

3.4. Analysis of Propeller Hydrodynamic Performance for Different Model Ice Widths. In this section, the changes in propeller hydrodynamic performance were measured for model ice with length of 200 mm; widths of 80, 160, 200, and 280 mm; and thickness of 120 mm. The blockage height is h = 95 mm, and the coordinates of the model ice are x_i = 20 mm, y_i= 0 mm, and z_i = -35 mm. Figure 13 shows the curve of the propeller hydrodynamic performance and amplification of propeller thrust and torque coefficients.

Figure 13 shows that the influence of varying model ice width on the propeller thrust is small at low advance coefficients. However, the propeller torque is greater for wider

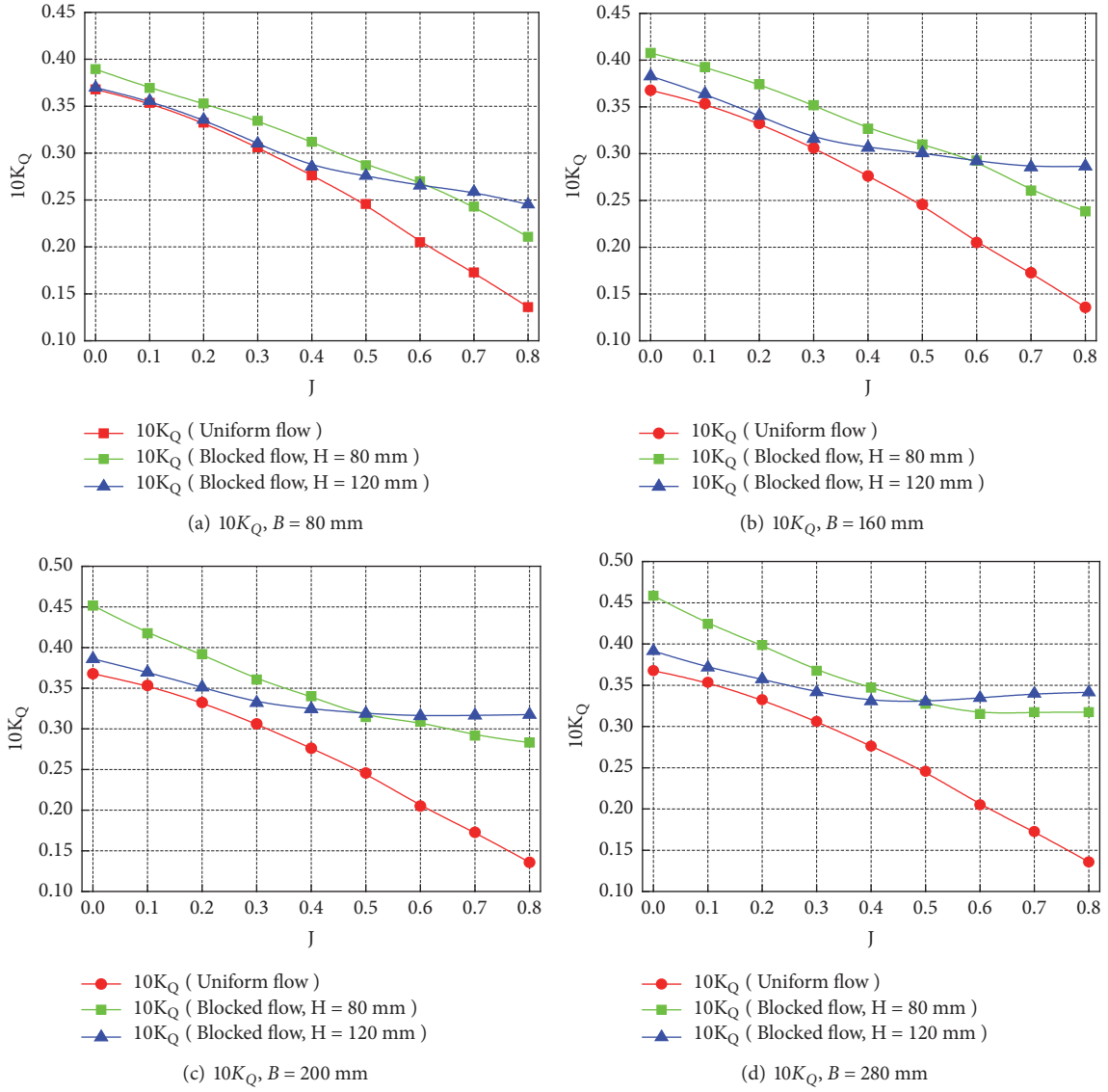

Figure 9: Variation of propeller torque coefficient with different model ice thicknesses.

model ice. As the advance coefficient increases, the thrust and torque under blocked flow decrease linearly. For 80 mm width, the trends of the thrust and torque coefficients are the same as those for a propeller in open water. For width of 160-280 mm and high advance coefficient, the thrust and torque tend to be stable. In addition, the figure shows that the thrust and torque gentle faster for wider model ice. For low advance coefficient, the change in model ice width has no effect on propeller efficiency. As the advance coefficient increases, for 80 mm model ice width, the propeller efficiency linearly increases and then gradually decreases in a manner similar to that of a propeller in open water. For model ice width of 160 mm $\leq B \leq$ 280 mm, the change in model ice width has no effect on the propeller efficiency. As the advance coefficient increases, the trends linearly increase with the advance coefficient, and for high advance coefficients, the propeller efficiency exceeds 90%. Moreover, in Figure 13(d), the amplification of the thrust coefficient and torque coefficient increased continuously with the advance coefficient, and the fastest increase occurred at high advance coefficient. At the same time, the wider the model ice, the greater the amplification of the thrust and torque coefficients, and the amplification of the thrust coefficient was greater than that of the torque coefficient.

3.5. Analysis of Propeller Hydrodynamic Performance for Different Quantities of Model Ice. The ice-going ship sails through level ice, pack ice channels, and ice floe zones. In particular, the ice-going ship operates astern in ice-breaking mode, and different quantities of ice gradually approach the propeller along the hull and cause the propeller to be affected, leading to considerable changes in the propeller hydrodynamic performance [24–26]. Considering the installation space of the experimental device, propeller scale, and

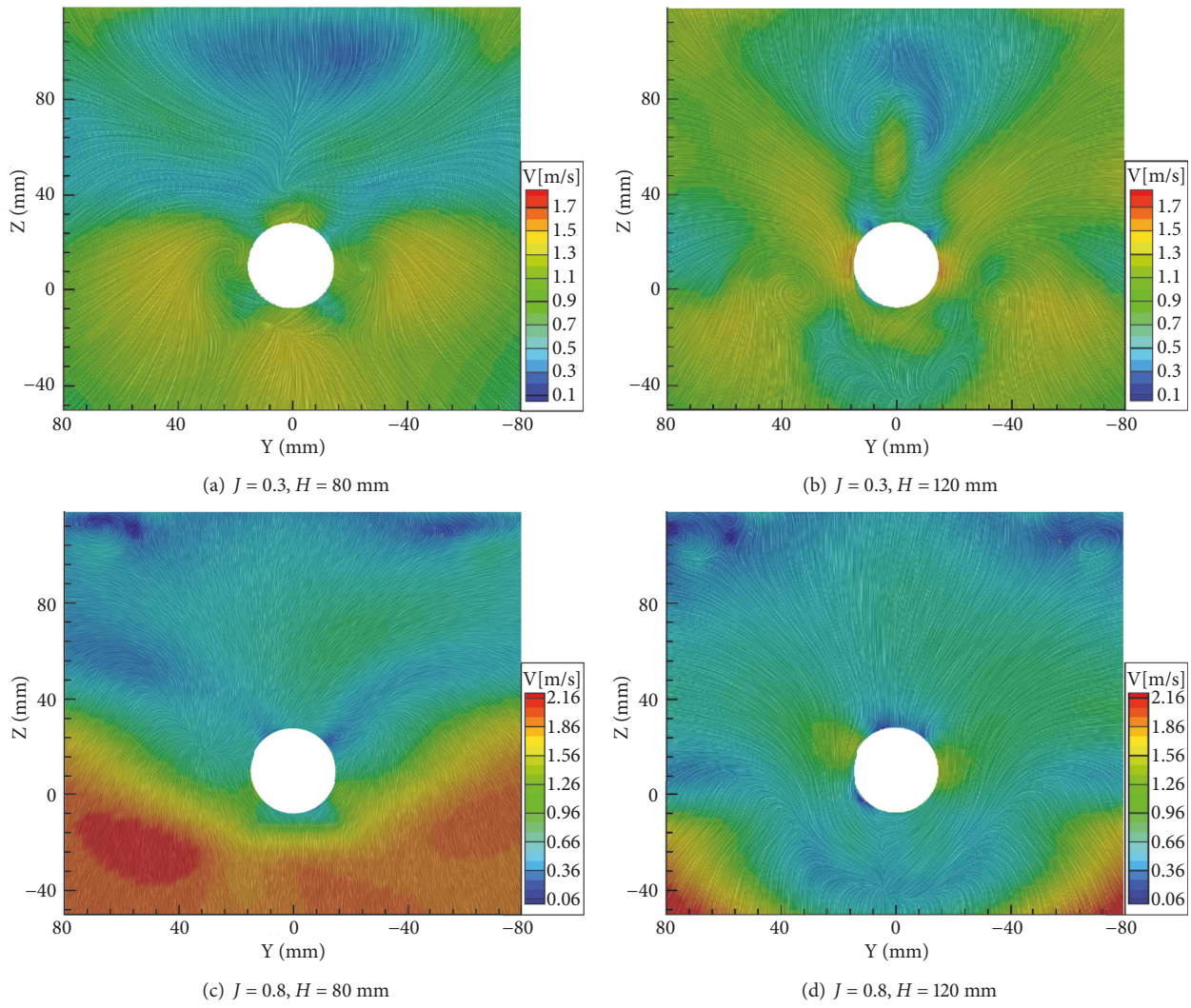

(a) $J = 0.3$, $H = 80$ mm

(b) $J = 0.3$, $H = 120$ mm

(c) $J = 0.8$, $H = 80$ mm

(d) $J = 0.8$, $H = 120$ mm

Figure 10: Velocity vector chart of the cross section between the propeller and the model ice.

other factors, the effects of one, two, and three pieces of ice in the blockage condition on the propeller hydrodynamic performance are studied. Figure 14 shows the blockage heights and installation position of the model ice. The model ice had length of 200 mm, width of 80 mm, and thickness of 80 mm; i is the model ice reference point; and the blockage heights of the propeller are $h = 35$ and 55 mm. The coordinates of the model ice are $x_i = 20$ mm, $y_i = 0$ mm, $z_i = 5$ mm; $x_i = 20$ mm, $y_i = \pm 60$ mm, $z_i = -35$ mm; and $x_i = 20$ mm, $y_i = 0$ mm, $z_i = -135$ mm. Figure 15 shows the curve of the propeller hydrodynamic performance and the amplification of the propeller thrust and torque coefficients.

Figure 15 clearly shows that the greater the number of pieces of model ice, the greater the effect on the thrust and torque of the propeller. For one piece of model ice, the thrust and torque coefficients decrease linearly with an increase in the advance coefficient and the propeller efficiency linearly increases and then decreases gradually in a manner similar to a propeller in open water. When two pieces of model ice have a blockage effect on the propeller, the thrust and torque coefficients initially decrease at a rate similar to that in the case of one piece and then start to gentle, and the propeller efficiency linearly increases. When three pieces of model ice have a blockage effect on the propeller, the propeller thrust and torque coefficients decrease linearly and at high advance coefficient, the propeller thrust increases gradually and the torque decreases suddenly. This is mainly due to the high advance coefficient resulting in the greater inflow velocity and the ice blockage becoming more obvious, resulting in a significant increase in the pressure of the propeller blade surface in the blocked zone and a significant decrease in pressure at the back of the blade [15]. Owing to the increase in the number of ice blocks, the number of vortices between the propeller and the model ice increases, and therefore, the velocity gradient around the propeller blades decreases rapidly and the friction resistance of the propeller blades decreases, resulting in a decrease in the propeller torque.

Furthermore, when three pieces of model ice have a blockage effect on the propeller, the propeller efficiency linearly increases at first and then increases more rapidly,

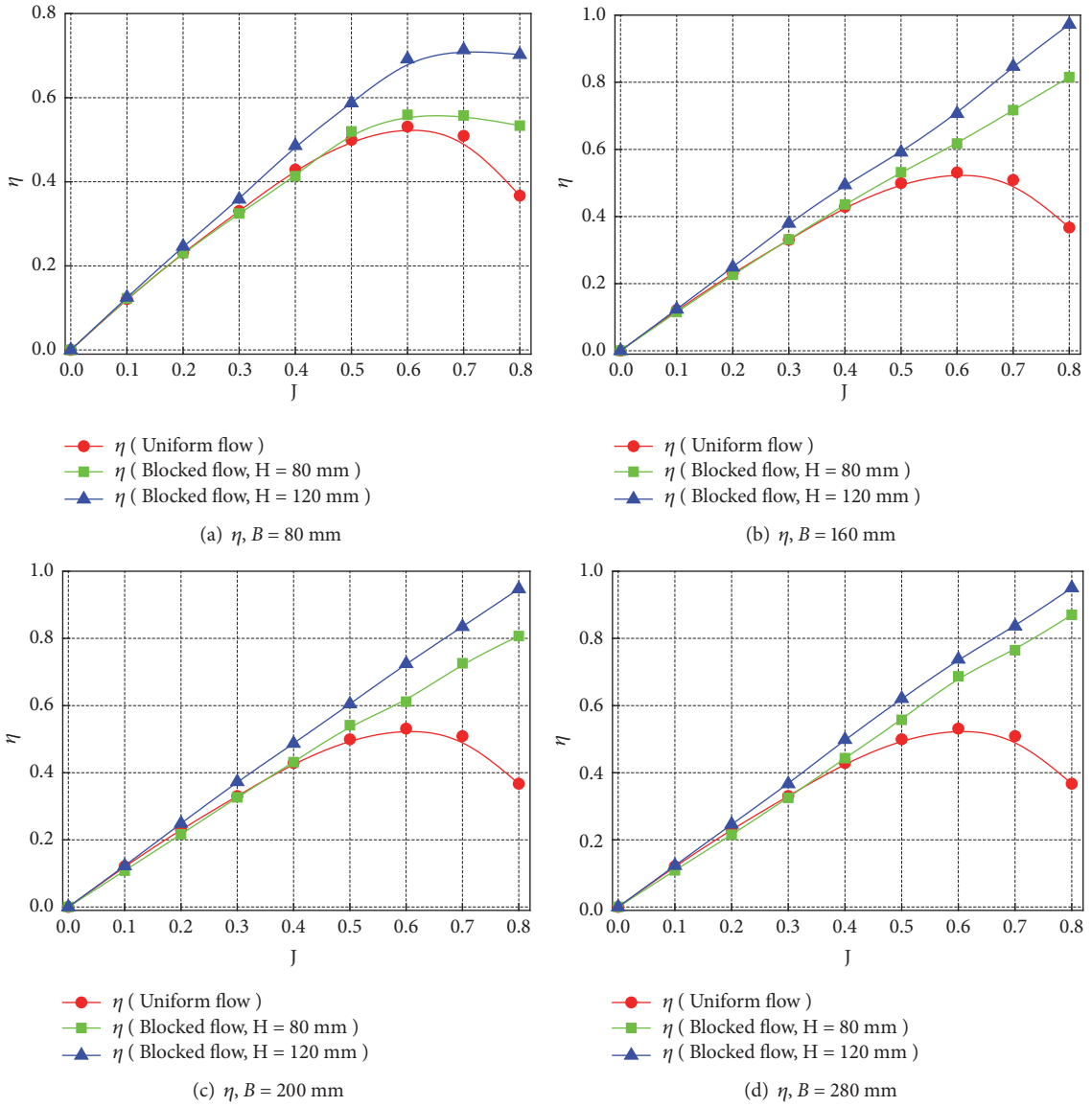

Figure 11: Variation of propeller efficiency with different model ice thicknesses.

and the propeller efficiency exceeds 100% at high advance coefficient. This is mainly the result of the amplification of the propeller thrust and torque and exaggerated inflow velocity in front of the propeller. The figure shows that, for low advance coefficient, the varying number of ice pieces has no influence on the propeller efficiency, and the propeller efficiency is equal to that of a propeller in open water. For high advance coefficient, the more the number of model ice pieces, the larger the effect on propeller efficiency. Figure 15(d) also shows that, for low advance coefficient, the amplification of the propeller thrust and torque coefficients is minimally affected by the number of ice pieces. With an increase in the advance coefficient and number of ice pieces, the amplification of the propeller thrust and torque coefficients increases, and the amplification of the thrust coefficient is greater than that of the torque coefficient. Furthermore, the difference between the propellers thrust and torque coefficient amplifications also increases. When three pieces of model ice have a blockage effect on the propeller, the difference between the amplification of the thrust coefficient and that of the torque coefficient reaches its maximum. In this case, the amplification of the thrust coefficient increased to 600% and that of the torque coefficient increased to 160%; thus, the efficiency of the propeller in blockade flow reached its maximum.

3.6. Analysis of Flow Field Characteristics. In the experiments described in this section, model ice blockages with length of 200 mm; widths of 80, 160, 200, and 280 mm; and thickness of 80 mm were selected as the research objects. The initial coordinates of the model ice are $x_i = 20$ mm, $y_i = 0$ mm, and $z_i = 5$ mm. First, the propeller wake flow field in the open-water test was measured. Then, the propeller wake flow field was measured for four different widths of model ice, and the

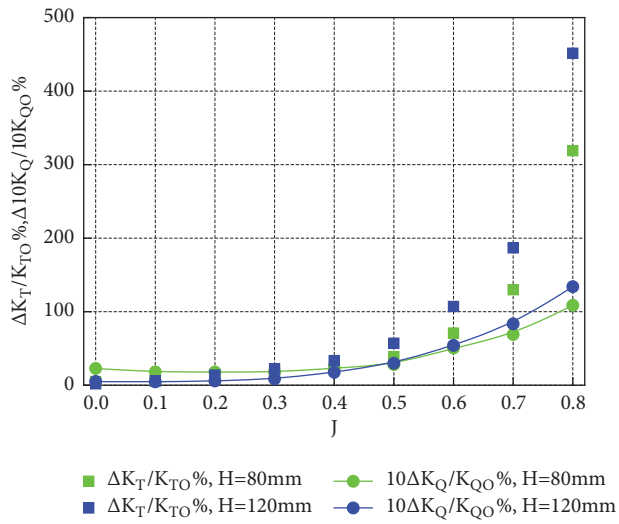

Figure 12: Variation of the amplification of the propeller thrust and torque coefficients with different model ice thicknesses.

propeller wake flow field for advance coefficient of $J = 0.4$ ($V_A = 1$ m/s) was analyzed. The plane located at $X = -50$ mm from the coordinate origin was selected as the measurement surface, as shown in Figures 16 and 17(a) and Figure 16 shows the schematic diagram of the experimental setup with the PIV system.

The experimental process and PIV stereo imaging system need to be photographed and analyzed using two charge-coupled device (CCD) cameras. However, the inclined rear camera was blocked by the propeller shaft, and this created a visual blind spot when the camera was capturing images. During postprocessing, the system was unable to recognise the blind spot. In Figure 17(b), this region is marked with a red ellipse (this marking is not shown in the other graphs). In addition, the data presented are observed from the propeller shaft toward the inflow direction. In Figure 17(e), model ice with $B = 280$ mm cannot be fully displayed because the model ice width is large; thus, green ellipses are used to represent the ice. Based on the sheltering zone of the propeller shaft in Figure 17, green boxes are added to Figures 18 and 19 to represent the sheltering zone of the propeller shaft. Figures 17, 18, and 19 show the velocity contours in the three directions of the propeller wake field.

Figure 17 shows that, for an open-water test of the propeller, the velocity gradient of the entire flow field in the cross section is clear, showing a trend of gradual increase and decrease from the inside to the outside. The velocity at the propeller blade tip is basically the same as the trailer velocity ($V_A = 1$ m/s), as indicated by the accuracy of the measurement results. A high-velocity zone is generated at $0.5R$ of the propeller blade, and a high-velocity zone appears in the local area below the propeller, as shown in Figure 17(b). A comparison of the velocity contours of the propeller in open water and blocked flow indicates that the fluid velocity in the cross section of the propeller clearly decreases. The main reason is the blockage effect of the model ice that reduces the inflow velocity before the propeller and causes a decrease in the velocity of the propeller wake flow field. Moreover, the velocity on the left is still higher than that on the right in the blocked region. In the unblocked region, the velocity of the propeller wake flow field is reduced; however, there is still a more obvious high-velocity zone under the propeller. When the model ice width is 80 mm $\leq B \leq$ 200 mm, the velocity gradient in the cross section is clear and shows a trend of gradual increase and decrease from the inside to the outside. When the model ice width is $B = 280$ mm, the flow field in the cross section is turbulent. The figure shows that the fluid velocity clearly changes from the blade root to $0.5R$ and that the flow velocity decreases and the change is more uniform from $0.5R$ to the blade tip position. The comparison also indicates that as the model ice gets wider, the blockage region increases, flow velocity of the propeller wake flow along the x-axis decreases, and turbulence of the flow field increases.

Figure 18 shows the velocity contours of the wake flow field section of the propeller on the y-axis under both open-water and blocked conditions. In the figure, the velocities in the positive and negative directions along the y-axis are, respectively, indicated in yellow and blue. Figure 18 indicates that, for propeller operation in the open-water test, the velocity in the negative direction of the y-axis is located directly below the cross section and between the blade root and $0.75R$. The velocity in the positive direction of the y-axis is located at the upper end of the section; this agrees with the manifestation of flow field velocity when the propeller is revolving in the left direction. When the propeller is blocked by model ice, the velocity regions in the positive and negative directions of the y-axis, respectively, increase at the upper and lower ends of the cross section. Simultaneously, the velocity field in the cross section becomes more turbulent than that in the open-water section. This is mainly due to model ice in the front of the propeller that makes the inflow before the propeller more turbulent and accelerates the increase in the velocity component in the y-direction. In addition,

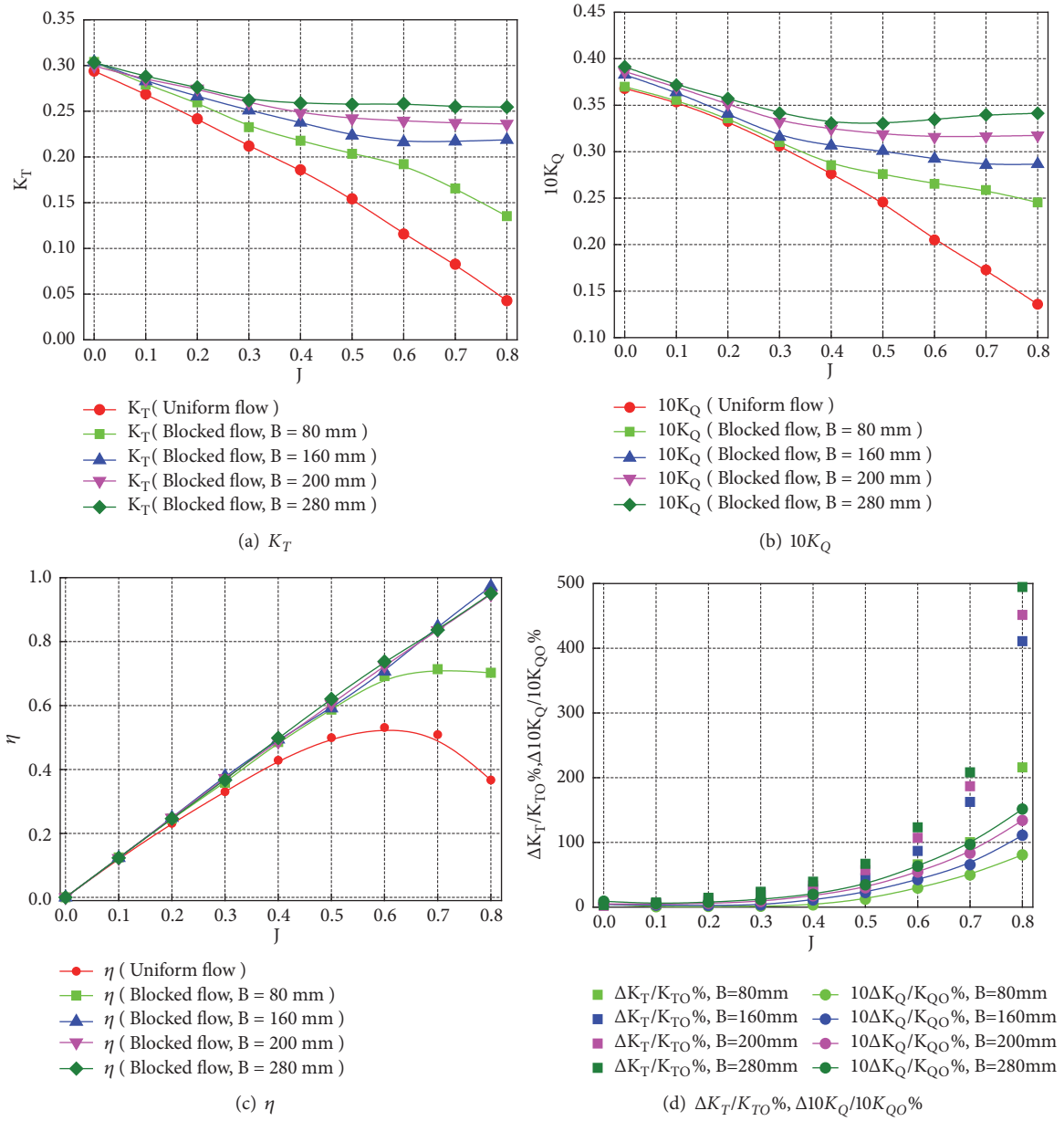

Figure 13: Variation of the propeller hydrodynamic performance and amplification of propeller thrust and torque coefficients with different model ice widths.

owing to the blockage effect of model ice on the propeller, the velocity region area of the propeller in the positive and negative directions of the y-axis also increases. The figure shows that when model ice becomes increasingly wider, the increase in the positive direction of the y-axis velocity region at the upper end of the cross section becomes increasingly obvious. By contrast, the negative direction of the y-axis at the lower end of the section shows a gradually decreasing trend.

Figure 19 shows the velocity contours of the wake flow field section of the propeller on the z-axis under both open-water and blocked conditions. In the figure, the velocities in the positive and negative directions along the z-axis are, respectively, indicated in yellow and blue. Figure 19(a) shows that when the propeller is in the open-water test, the z-axis negative direction velocity zone on the left side of the section is quite apparent (this zone generates two upper and lower parts because of the obstruction of the propeller shaft) and is mainly concentrated between the blade root and $0.75R$, and the closer the location to the propeller shaft, the greater the negative direction velocity of the z-axis. The right side of the section is the z-axis positive direction velocity zone that is mainly located near the blade root. The velocity distribution of the propeller wake flow field in the direction of the z-axis is in accordance with the rotation direction of the propeller. When the propeller is blocked with model ice, the z-axis positive velocity zone on the right side of the section moves

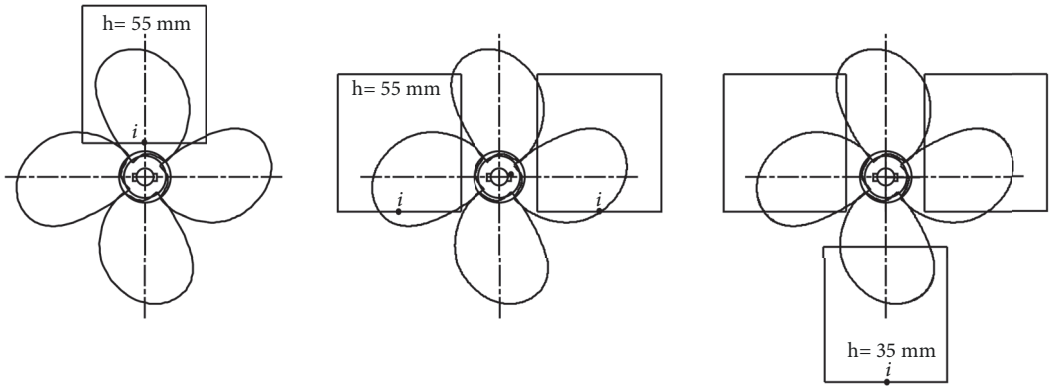

x_i = 20 mm, y_i = 0 mm, z_i = 5 mm; x_i = 20 mm, y_i = ± 60 mm, z_i = - 35 mm; x_i = 20 mm, y_i = 0 mm, z_i = - 135 mm

Figure 14: Schematic diagram of model ice blockage heights and installation position.

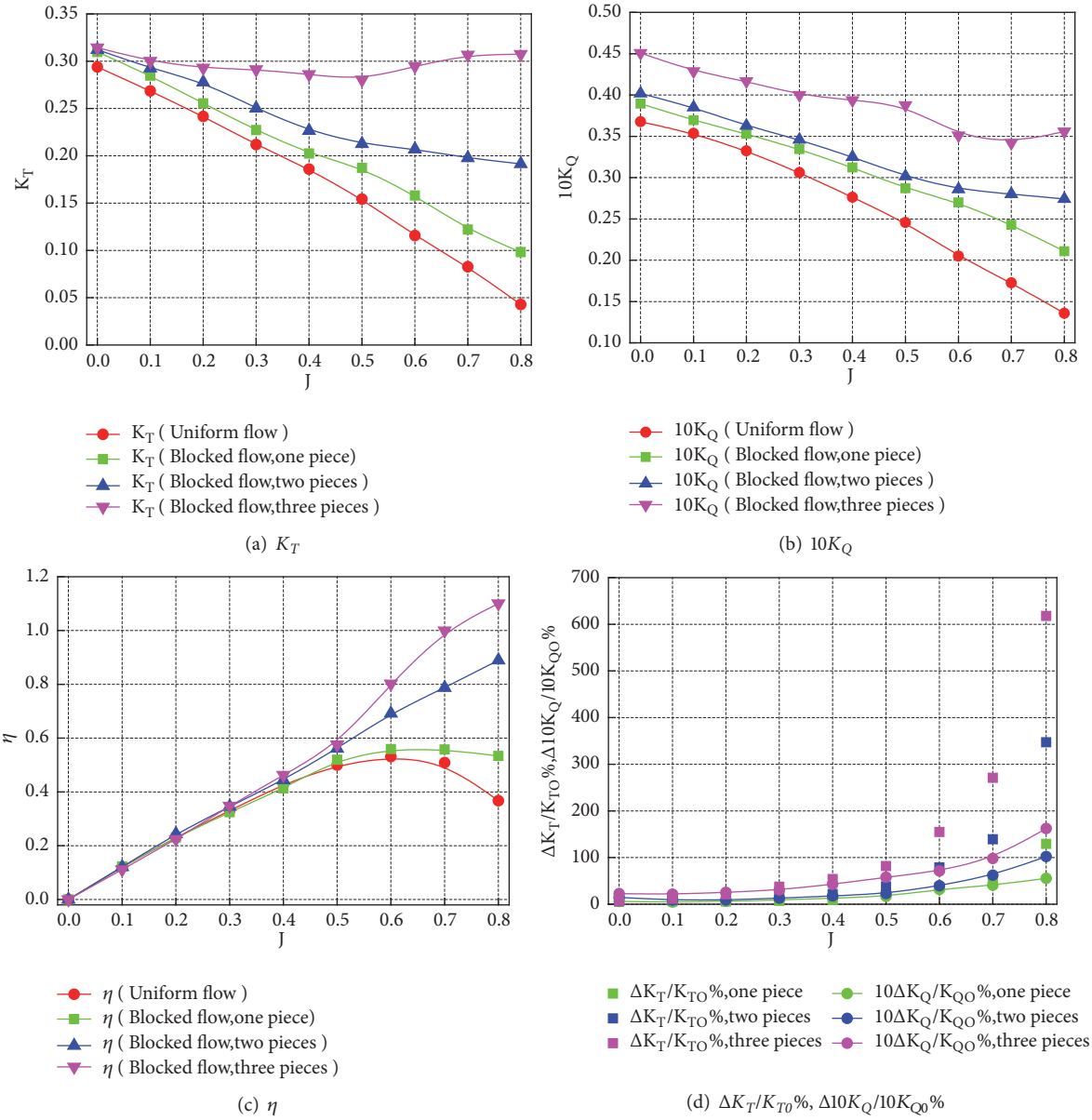

(a) K_T

(b) $10K_Q$

(c) η

(d) $\Delta K_T/K_{T0}$%, $\Delta 10K_Q/10K_{Q0}$%

Figure 15: Variation of the propeller hydrodynamic performance and amplification of the propeller thrust and torque coefficients with different numbers of ice pieces.

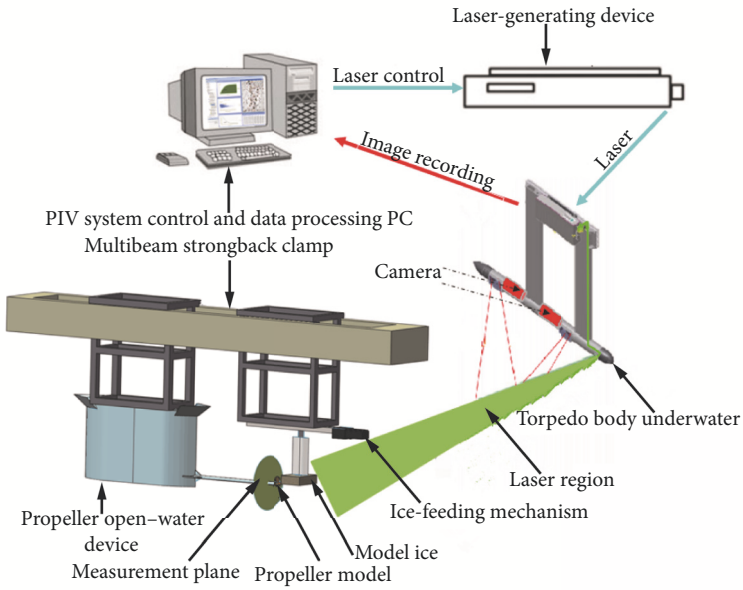

Figure 16: Schematic diagram of experimental setup with PIV system.

gradually toward the blade tip direction and is gradually divided into two parts. The z-axis positive direction velocity region shows a gradually increasing trend as the model ice width increases, and the upper velocity region increases at a faster rate. As the model ice width increases, the z-axis negative velocity region at the upper and lower ends of the left section gradually varies. When the model ice width is 80-160 mm, the z-axis negative direction velocity region at the left upper end of the section shows a gradually increasing trend. When the model ice width is 200-280 mm, this zone gradually decreases. When the model ice width is B = 280 mm, the z-axis negative direction velocity region at the upper end is smaller than that when the propeller is in open water. The z-axis negative velocity region at the left lower end of the section shows a decreasing trend as the model ice width increases.

To analyze the main causes of this phenomenon, the wake flow fields for four different model ice widths are analyzed, with the measurement section located 20 mm after the model ice. The model ice had length of 200 mm; widths of 80, 160, 200, and 280 mm; and thickness of 80 mm. The advance coefficient is J = 0.4 (V_A = 1 m/s). The installation position and velocity of the model ice are the same as those described above; the only difference is that the wake flow field information of the model ice was measured, and the propeller and open-water experimental device were not on the trailer. After the test, the velocity contours along the z-axis in the section were generated, as shown in Figure 20. The figure shows that there is a great difference in the change trend of the flow field with varying widths. As the model ice width increases, the fluid velocity in the negative direction of the z-axis in the cross section decreases and the effect on the fluid velocity in the front z-direction of the propeller decreases. Therefore, it can be proved in Figure 19 that the velocity contours on the z-axis in the cross section during propeller-ice interaction. As the model ice width increases, the positive direction velocity region of the z-axis on the right side of the section increases gradually, and the negative direction velocity region of the z-axis on the left side of the section depends on the model ice width.

4. Conclusions

This paper studies the influence of the sizes, quantities, and axial positions of synthetic ice on the propeller hydrodynamic performance in a ship model towing tank. Concurrently, Particle Image Velocimetry (PIV) is used to analyze the blocked flow field of the propeller.

The main conclusions of this paper are as follows:

(1) The blockage leads to an increase in propeller thrust, torque, and efficiency. The increase in thrust and torque can be attributed to combined action of the blockage effect and the wall effect, while the increase in propeller efficiency is mainly due to the thrust coefficient rising faster than the torque coefficient. By analyzing the relationship between the degree of blockage and the advance coefficient, it is found that the smaller the advance coefficient of the propeller, the smaller the influence of model ice on propeller blockage.

(2) Given an advance coefficient and position, the thicker the model ice, the greater its effect on the thrust and efficiency of the propeller. At low advance coefficient, the propeller torque is larger when the model ice is thinner and lower when the model ice is thicker. This is attributed to the vortex formed between the propeller and the model ice. At high advance coefficient, however, the effect of model ice on propeller torque is the opposite to the low advance coefficient, as no vortex is formed between the propeller and the model ice.

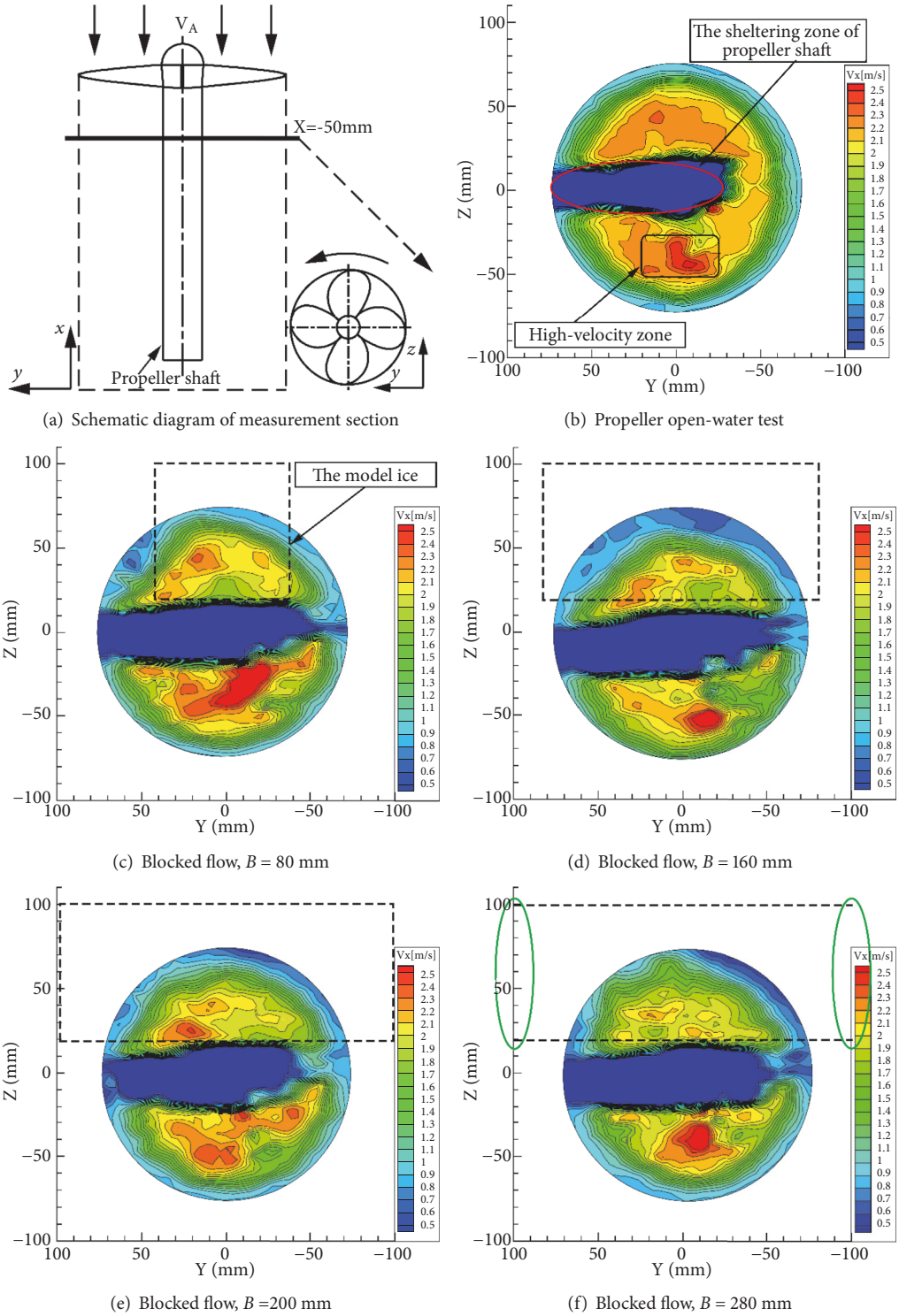

(a) Schematic diagram of measurement section

(b) Propeller open-water test

(c) Blocked flow, B = 80 mm

(d) Blocked flow, B = 160 mm

(e) Blocked flow, B =200 mm

(f) Blocked flow, B = 280 mm

Figure 17: Velocity contours of propeller wake flow field along x-axis.

(3) At a fixed advance coefficient and position, the wider the model ice, the greater its effect on the propeller thrust and torque. In terms of the effect on propeller efficiency, when the width of the model ice exceeds the propeller diameter, there is no effect on the propeller hydrodynamic performance. When different amounts of model ice interact with the propeller, the larger the number of model ice interacting with the propeller, the larger the effect on the thrust and torque of the propeller. In terms of the effect on the efficiency of the propeller, it can be concluded that, at low advance coefficients, different

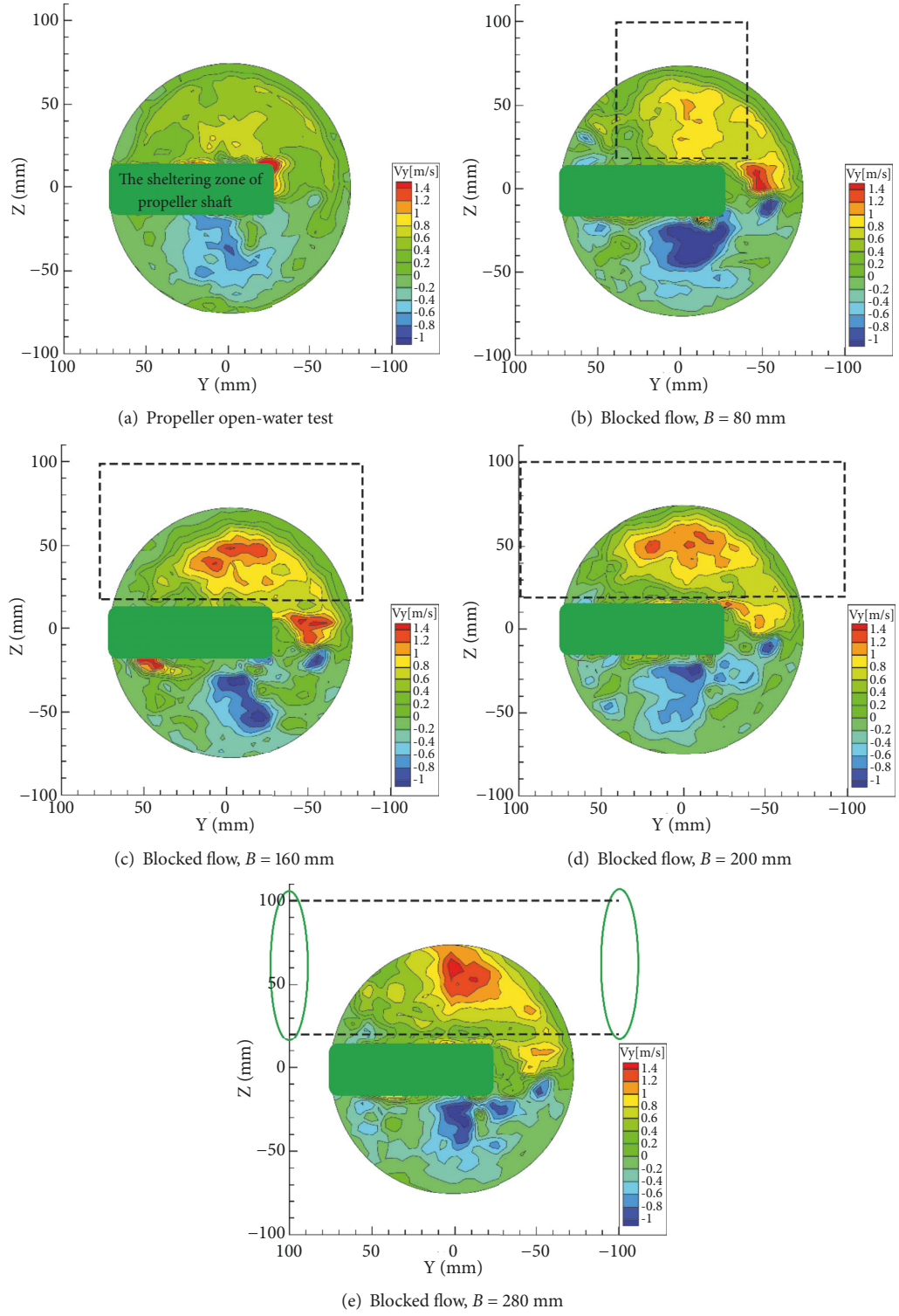

(a) Propeller open-water test

(b) Blocked flow, $B = 80$ mm

(c) Blocked flow, $B = 160$ mm

(d) Blocked flow, $B = 200$ mm

(e) Blocked flow, $B = 280$ mm

Figure 18: Velocity contours of propeller wake flow field along y-axis.

amounts of model ice do not affect the propeller efficiency. At high advance coefficients, the more the model ice, the higher the propeller efficiency.

(4) By comparing the flow field characteristics of the propeller using PIV technology, it is found that, compared to the case where the propeller is in open water, the flow velocity of the wake flow is reduced in the inflow direction when the propeller is blocked with model ice. In addition, the fluid velocity increases in both the horizontal transverse directions and the positive vertical direction, while the change in fluid

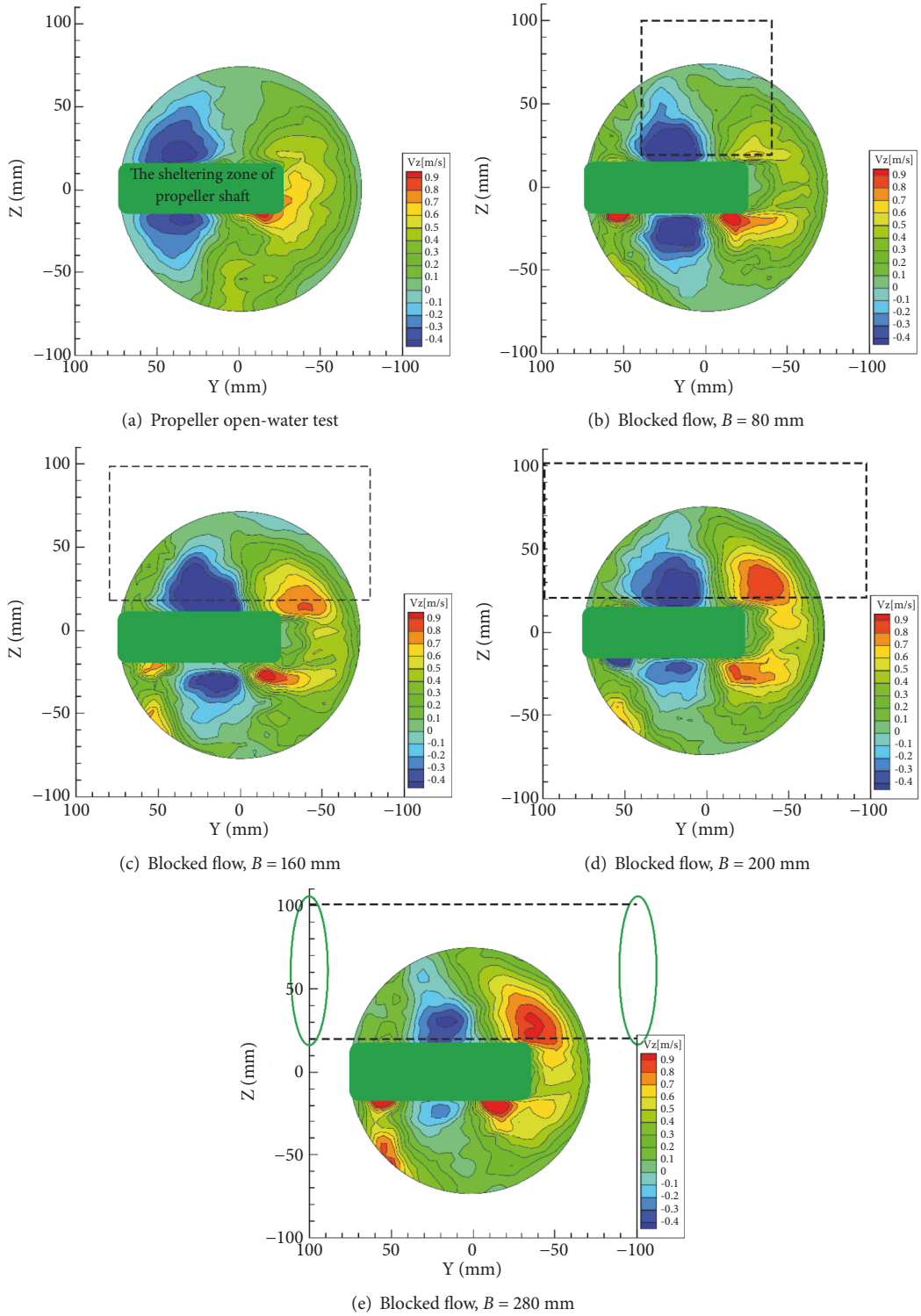

(a) Propeller open-water test

(b) Blocked flow, $B = 80$ mm

(c) Blocked flow, $B = 160$ mm

(d) Blocked flow, $B = 200$ mm

(e) Blocked flow, $B = 280$ mm

Figure 19: Velocity contours of propeller wake flow field along z-axis.

velocity in the negative vertical direction is related to the width of model ice.

This study investigates the influence of different sizes, numbers, and axial positions of model ice on the propeller hydrodynamic performance. The regular patterns and mechanisms of propeller-ice interaction are obtained to provide support and reference for experimental research, theoretical methods, potential flow theory, and numerical simulations of propeller-ice interaction. Follow-up work will be completed to include milling experiments on the propeller-ice interaction and experiments on the free motion of ice under the suction of a propeller. In the propeller-ice milling

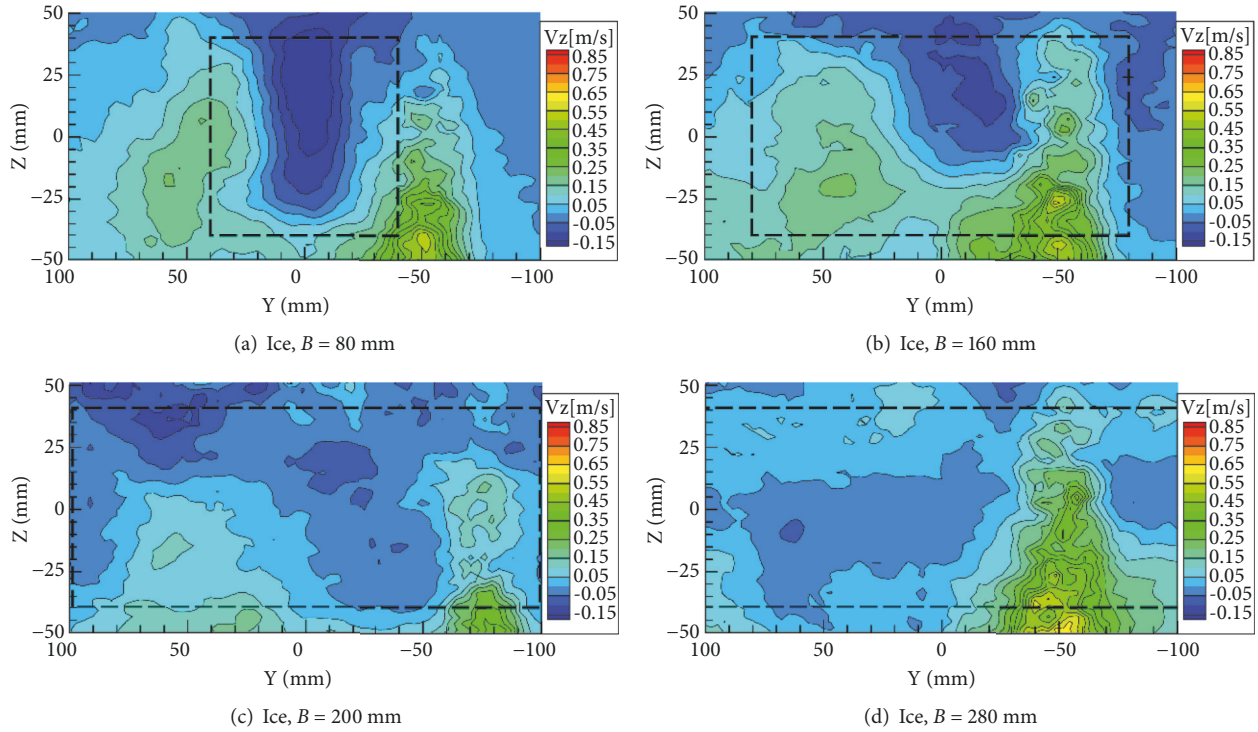

(a) Ice, $B = 80$ mm

(b) Ice, $B = 160$ mm

(c) Ice, $B = 200$ mm

(d) Ice, $B = 280$ mm

Figure 20: Velocity contour of the cross section of four different model ice widths along the z-axis.

and impact processes, the load components, size, and pulse characteristics at different positions on the blade surface will be investigated.

Data Availability

The data used to support the findings of this study are available from the corresponding author upon request.

Conflicts of Interest

The authors declare that there are no conflicts of interest regarding the publication of this paper.

Acknowledgments

The research described in this paper was financially supported by the National Natural Science Foundation of China (Grants nos. 51679052, 51639004, and 51809055), the Defense Industrial Technology Development Program (Grant no. JCKY2016604B001), and the Natural Science Foundation of Heilongjiang Province of China (Grant no. E2018026).

References

[1] H. Lindroos and H. Bjorkestam, "Hydrodynamic loads developed during ice-clogging of a propeller nozzle and means to prevent the clogging," in *Proceedings of the International Offshore and Navigation Conference and Exhibition*, Helsinki, Finland, 1986.

[2] V. S. Shpakoff and H. Segercrantz, "On the influence of different operating conditions on the level of external ice forces on the propeller-shaft system of a single-screw ship," *International Shipbuilding Progress*, vol. 32, no. 368, pp. 86–91, 1985.

[3] L. Luznik, D. Walker, N. Bose, and S. J. Jones, "Effects of ice blockage size and proximity on propeller performance during non-contact propeller-ice interaction," in *Proceedings of the 14th International Conference on Offshore Mechanics and Arctic Engineering. Part 5 (of 5)*, pp. 35–39, Copenhagen, Denmark, June 1995.

[4] S. Newbury, L. Shih, and R. Browne, "Experimental and theoretical evaluation of hydrodynamic pressure during non-contact propeller/ice interaction," in *Proceedings of the in Proceedings of the 2nd Canadian Marine Dynamics Conference*, Vancouver, Canada, 1993.

[5] S. Newbury, R. Browne, and S. Jones, "Experimental determination of hydro-dynamic non-contact loads during propeller ice interaction," in *Proceedings of the in Proceedings of the 4th International Offshore and Polar Engineering Conference*, Osaka, Japan, 1994.

[6] D. Walker, H. Bose, and H. Yamaguchi, "Hydrodynamic performance and cavitation of an open propeller in a simulated ice-blocked flow," *Journal of Offshore Mechanics and Arctic Engineering*, vol. 116, no. 3, pp. 185–189, 1994.

[7] C. Moores, B. Veitch, N. Bose, S. Jones, and J. Carlton, "Multi-component blade load measurements on a propeller in ice," *Transactions - Society of Naval Architects and Marine Engineers*, vol. 110, pp. 169–187, 2003.

[8] R. Sampson, M. Atlar, and N. Sasaki, "Effect of cavitation during systematic ice block tests," in *Proceedings of the 19th International Conference on Port and Ocean Engineering under Arctic Conditions*, pp. 372–383, Dalian, China, June 2007.

[9] R. Sampson, M. Atlar, J. W. St. John, and N. Sasaki, "Podded propeller ice interaction in a cavitation tunnel," in *Proceedings of*

the 3rd International Symposium on Marine Propulsors (SMP13), Tasmania, Australia, 2013.

[10] J. Wang, *Prediction of propeller performance on a model podded propulsor in ice [Ph.D. thesis]*, Memorial University of Newfoundland, Newfoundland, Canada, 2007.

[11] L. Y. Shih and Y. Zheng, "Constricted hydrodynamic flow due to proximate ice blockage over a blade profile in 2-D," in *Proceedings of the in Proceedings of the 2nd International Symposium on Propeller and Cavitation*, Hangzhou, China, 1992.

[12] P. Liu, J. M. Doucet, B. Veitch, I. Robbins, and N. Bose, "Numerical prediction of ice induced hydrodynamic loads on propellers due to blockage," *Ocean Engineering*, vol. 4, no. 1, pp. 31–38, 2000.

[13] P. Liu, B. Colbourne, and C. Shin, "Prediction of transient loading on a propeller from an approching ice block," *Journal of Naval Architecture and Marine Engineering*, vol. 2, no. 1, 2009.

[14] P. Liu, A. Akinturk, M. He, M. F. Islam, and B. Veitch, "Hydrodynamic performance evaluation of an ice class podded propeller under ice interaction," in *Proceedings of the 27th International Conference on Offshore Mechanics and Arctic Engineering, OMAE 2008*, pp. 21–29, Germany, June 2008.

[15] C. Wang, S. X. Sun, X. Chang, and L. Y. Ye, "Numerical simulation of hydrodynamic performance of ice class propeller in blocked flow–using overlapping grids method," *Ocean Engineering*, vol. 141, pp. 418–426, 2017.

[16] D. Walker, N. Bose, H. Yamaguchi, and S. J. Jones, "Hydrodynamic loads on ice-class propellers during propeller-ice interaction," *Journal of Marine Science and Technology*, vol. 2, no. 1, pp. 12–20, 1997.

[17] M. Atlar, I. Prasetyawan, W. D. Aryawan, D. Wang, and N. Sasaki, "Cavitation in ice-milling with a podded propulsor," in *Proceedings of the 4th ASME/JSME Joint Fluids Engineering Conference*, pp. 269–278, USA, July 2003.

[18] ITTC-Recommended Procedures, "Propulsion Performance-Podded Propeller Tests and Extrapolation 7.5-02-03-01.3," 2002.

[19] J. Seo, S. J. Lee, B. Han, and S. H. Rhee, "Influence of design parameter variations for propeller-boss-cap-fins on hub vortex reduction," *Journal of Ship Research*, vol. 60, no. 4, pp. 203–218, 2016.

[20] C. Wang, L. Y. Ye, X. Chang, and X. Li, "Test of hydrodynamic loads under non-contact propeller-ice interaction," *Harbin Gongcheng Daxue Xuebao/Journal of Harbin Engineering University*, vol. 38, no. 8, pp. 1190–1196, 2017.

[21] J. M. Doucet, *Cavitation erosion experiments in blocked flow with two ice-class propeller models [Ph.D. thesis]*, Memorial University of Newfoundland, Newfoundland, Canada, 1996.

[22] D. Polić, S. Ehlers, and V. Æsøy, "Propeller torque load and propeller shaft torque response correlation during ice-propeller interaction," *Journal of Marine Science and Application*, vol. 16, no. 1, 2017.

[23] Z. B. Sheng and Y. Z. Liu, "Watercraft principle: ship propulsion," in *Open Water Test of Propeller Model*, vol. 4, Chapter 4, pp. 35-36, 2004.

[24] S. Van Der Werff, J. Brouwer, and G. Hagesteijn, "Ship resistance validation using artificial ice," in *Proceedings of the ASME 2015 34th International Conference on Ocean, Offshore and Arctic Engineering, OMAE 2015*, Newfoundland, Canada, June 2015.

[25] I. Metrikin, S. Kerkeni, P. Jochmann, and S. Løset, "Experimental and numerical investigation of dynamic positioning in level ice," *Journal of Offshore Mechanics and Arctic Engineering*, vol. 137, no. 3, 2015.

[26] M. Tikanmaki, J. Heinonen, and A. Kinnunen, "Comparison of ice load models for azimuthing thruster ice load calculation," *AZIRULE*.VTT-R-10310-10, 2010.